Exploiting the Pyrazolo[3,4-*d*]pyrimidin-4-one Ring System as a Useful Template To Obtain Potent Adenosine Deaminase Inhibitors

Concettina La Motta,*,[†] Stefania Sartini,[†] Laura Mugnaini,[†] Silvia Salerno,[†] Francesca Simorini,[†] Sabrina Taliani,[†] Anna Maria Marini,[†] Federico Da Settimo,[†] Antonio Lavecchia,[§] Ettore Novellino,[§] Luca Antonioli,[‡] Matteo Fornai,[‡] Corrado Blandizzi,[‡] and Mario Del Tacca[‡]

Dipartimento di Scienze Farmaceutiche, Università di Pisa, Via Bonanno, 6, 56126 Pisa, Italy, Dipartimento di Chimica Farmaceutica e Tossicologica, Università di Napoli "Federico II", Via D. Montesano, 49, 80131 Napoli, Italy, and Centro Interdipartimentale di Ricerche di Farmacologia Clinica e Terapia Sperimentale, Via Roma 55, 56126 Pisa, Italy

A number of pyrazolo[3,4-*d*]pyrimidin-4-ones bearing either alkyl or arylalkyl substituents in position 2 of the nucleus were synthesized and tested for their ability to inhibit adenosine deaminase (ADA) from bovine spleen. The 2-arylalkyl derivatives exhibited excellent inhibitory activity, showing K_i values in the nanomolar/subnanomolar range. The most active compound, 1-(4-((4-oxo-4,5-dihydropyrazolo[3,4-*d*]pyrimidin-2-yl)methyl)phenyl)-3-(4-(trifluoromethyl)phenyl)urea, **14d**, was tested in rats with colitis induced by 2,4-dinitrobenzenesulfonic acid to assess its efficacy to attenuate bowel inflammation. The treatment with **14d** induced a significant amelioration of both systemic and intestinal inflammatory alterations in animals with experimental colitis. Docking simulations of the synthesized compounds into the ADA catalytic site were also performed to rationalize the structure−activity relationships observed and to highlight the key pharmacophoric elements of these products, thus prospectively guiding the design of novel ADA inhibitors.

Introduction

Adenosine deaminase (adenosine aminohydrolase, ADA,[*a*] EC 3.5.4.4) is a 41 kDa zinc protein involved in purine metabolism. It catalyzes the irreversible hydrolytic deamination of adenosine and 2′-deoxyadenosine to inosine and 2′-deoxyinosine, respectively, thus regulating the endogenous levels of these nucleosides. In addition, it plays a pivotal role in the development of the lymphoid system.[1−5] The importance of ADA activity for the maturation and differentiation of immune functions is supported by the evidence that an inherited deficiency of this enzyme in human beings triggers a form of severe combined immunodeficiency disease (SCID), characterized by a serious lymphoid cell shortage, leading to both a reduced number of T cells and their altered response to mitogens or antigens. Therefore, ADA inhibition can induce an immunosuppressive status, which can be profitably exploited for the treatment of different types of cancer affecting the immune system, such as leukemia and lymphoma.[6−10] In keeping with this concept, the antitumor properties of two natural antibiotics, coformycin (CF, **1**, Chart 1) and 2′-deoxycoformycin (dCF, **2**, Chart 1), have been associated with their ability to exert a potent inhibition of ADA.[11−13]

By preventing the breakdown of endogenous adenosine, ADA inhibitors may also have a therapeutic potential for managing pathological processes involving site- or event-mediated adenosine release. With regard to inflammation, high concentrations of extracellular adenosine are generated as a consequence of cellular stress, damage, or release of proinflammatory mediators. Accumulated adenosine is then able to counteract inflammation via reduction of cytokine biosynthesis and neutrophil functions, thus preventing phagocytosis, generation of toxic oxygen metabolites, and cell adhesion. As the blockade of ADA activity may increase the concentration of adenosine at inflamed sites, ADA inhibitors might have therapeutic relevance as novel anti-inflammatory drugs endowed with limited adverse effects.[14−18]

Several compounds have been shown to inhibit ADA with various degrees of potency. They are generally grouped into two main classes designated as "transition-state inhibitors", and "ground-state inhibitors". CF, **1**,[19] and dCF, **2**,[20] are the most potent compounds in the first class, while erythro-9-(2-hydroxy-3-nonyl)adenine[21] ((+)-EHNA, **3**, Chart 1) belongs to the second one. Current "transition-state inhibitors" are bound to the enzyme so tightly that their activity is nearly irreversible, thus giving rise to serious toxic effects. Moreover, they suffer from unfavorable pharmacokinetics, which reduces their oral bioavailability. On the other hand, the rapid metabolism of "ground-state inhibitors", such as (+)-EHNA, allows a fast recovery of the enzyme activity, with poor therapeutic effects. For these reasons, research efforts in this area are currently focused on the development of novel ADA inhibitors able to combine potent, prolonged, and reversible activity with favorable pharmacokinetic properties.

In order to discover novel drug candidates for the treatment of inflammatory bowel diseases (IBD), our group has started a research program on ADA, disclosing a novel class of inhibitors derived from the 4-aminopyrazolo[3,4-*d*]pyrimidine ring system and designed as (+)-EHNA analogues. The lead compound **4**, (*R*)-4-amino-2-(2-hydroxy-1-decyl)pyrazolo[3,4-*d*]pyrimidine, proved to be a highly potent ADA inhibitor, showing a K_i value of 53 pM.[22] Moreover, when administered intraperitoneally to

* To whom all correspondence should be addressed. Phone: (+)390502219593. Fax: (+)390502219605. E-mail: lamotta@farm.unipi.it.
† Università di Pisa.
§ Università "Federico II" di Napoli.
‡ Centro Interdipartimentale di Ricerche di Farmacologia Clinica e Terapia Sperimentale.
a Abbreviations: ADA, adenosine deaminase; SCID, severe combined immunodeficiency disease; CF, coformycin; dCF, 2′-deoxycoformycin; EHNA, erythro-9-(2-hydroxy-3-nonyl)adenine; APP, (*R*)-4-amino-2-(2-hydroxy-1-decyl)pyrazolo[3,4-*d*]pyrimidine; IBD, inflammatory bowel disease; DNBS, 2,4-dinitrobenzenesulfonic acid; TNF-α, tumor necrosis factor-α; IL-6, interleukin-6; MDA, malondialdehyde; PPOs, pyrazolopyrimidinones; SARs, structure−activity relationships.

Chart 1. Adenosine Deaminase Inhibitors
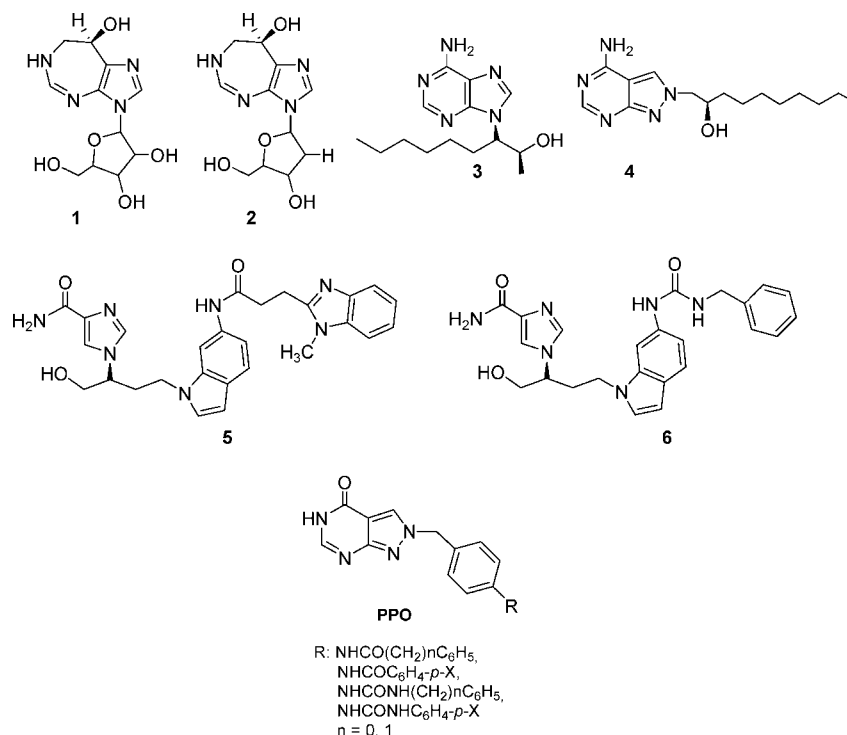
rats with colitis induced by 2,4-dinitrobenzenesulfonic acid (DNBS), **4** was found to attenuate both systemic and intestinal inflammatory parameters, improving macroscopic and histological features of colonic tissue and reducing levels of inflammatory mediators such as tumor necrosis factor-α (TNF-α), interleukin-6 (IL-6), and malondialdehyde (MDA).[23] In a subsequent step of our studies, we focused our attention on the novel, potent, and effective non-nucleoside inhibitors described by Terasaka and co-workers, **5** and **6** (Chart 1), exploiting the carboxamide moiety as a key framework for a fruitful and firm anchoring to the enzyme binding pocket.[24−28] Moving from these observations, we planned to change the 4-aminopyrazolo[3,4-*d*]pyrimidine heterocyclic core of our products into the pyrazolo[3,4-*d*]pyrimidin-4-one scaffold, thus developing a novel class of inhibitors as sterically constrained derivatives of **5** and **6**.

In the present article, we report the synthesis and the in vitro functional evaluation of a number of pyrazolopyrimidinones, PPOs, bearing either alkyl or arylalkyl substituents in position 2 of the nucleus. Compound **14d**, found to be the most active among all derivatives, was investigated in vivo for its anti-inflammatory activity in a rat model of IBD. Moreover, docking simulations of PPOs into the ADA catalytic site were carried out to propose their binding mode in the light of the structure−activity relationships (SARs).

Synthesis

The synthesis of the target inhibitors, **9a−c**, **13a−d,h**, and **14a−h**, was performed as outlined in Scheme 1. Alkylation of the commercially available 3-amino-4-pyrazolecarbonitrile, **7**, with the suitable alkyl bromides in DMF at 100 °C and in the presence of K_2CO_3 yielded the N^1-alkylpyrazoles **8a−c** as the main reaction products. Cyclization of **8a−c** with boiling formic acid provided the corresponding pyrazolo[3,4-*d*]pyrimidin-4-ones **9a−c**. Reaction of **7** with *p*-nitrobenzyl chloride gave the N^1-benzylpyrazole **10**, which was then converted to the pyrazolopyrimidinone **11** with boiling formic acid. Upon catalytic hydrogenation, performed under atmospheric pressure and room

temperature in the presence of Pd/C, **11** afforded the 2-(4-aminobenzyl)pyrazolo[3,4-*d*]pyrimidin-4-one **12**. The key intermediate **12** led to the desired inhibitors **13a−d,h** by reaction with the appropriate aroyl chloride in the presence of triethylamine and to inhibitors **14a−h** by treatment with the appropriate isocyanate, both protocols being carried out under microwave irradiation (Scheme 1).

Results and Discussion

Functional Evaluation. On the basis of a close parallel with the previously developed 4-aminopyrazolo[3,4-*d*]pyrimidines, APPs,[22] our program started with the synthesis of the inhibitors **9a−c**, bearing a *n*-nonyl, *n*-decyl, and *n*-undecyl chains, respectively, in position 2 of the heterocyclic core. Once tested for their efficacy against ADA from bovine spleen, these compounds did not show any appreciable inhibitory activity (Table 1), at variance with the parent APPs. Therefore, hypothesizing that the structural modification of the main scaffold could lead to a different interaction with the active site of the enzyme, we abandoned the substitution patterns of the prior series, focusing our attention toward bulkier substituents. Thus, we developed compounds **13a−d,h**, carrying an aroyl-aminoarylalkyl group in the same position 2 of the nucleus. As shown in Table 1, all the novel compounds were able to inhibit the in vitro activity of ADA, exhibiting K_i values in the nanomolar/subnanomolar range. In this subseries, the insertion of an electron-donating group in the para position of the distal phenyl ring did not affect significantly the inhibitory potency. Indeed, compound **13b**, bearing a methoxy function (K_i = 15.56 nM), was almost as potent as the unsubstituted parent compound **13a** (K_i = 12.65 nM). Conversely, the presence of an electron-withdrawing substituent in the same position of the pendent ring gave rise to a remarkable increase in potency. The insertion of a fluoro atom, as in **13c** (K_i = 0.96 nM), gave a 13-fold increase in inhibitory potency with respect to **13a**, while the presence of the bulkier trifluoromethyl group resulted in an even more remarkable increase in efficacy, and compound **13d**, with a K_i
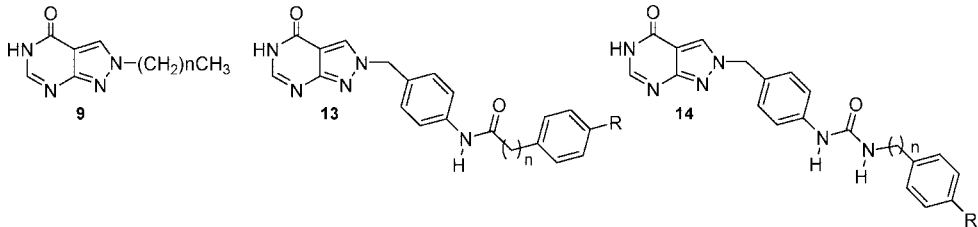
Scheme 1. Synthesis of Pyrazolo[3,4-*d*]pyrimidin-4-ones **9a**−**c**, **13a**−**d,h**, and **14a**−**h**
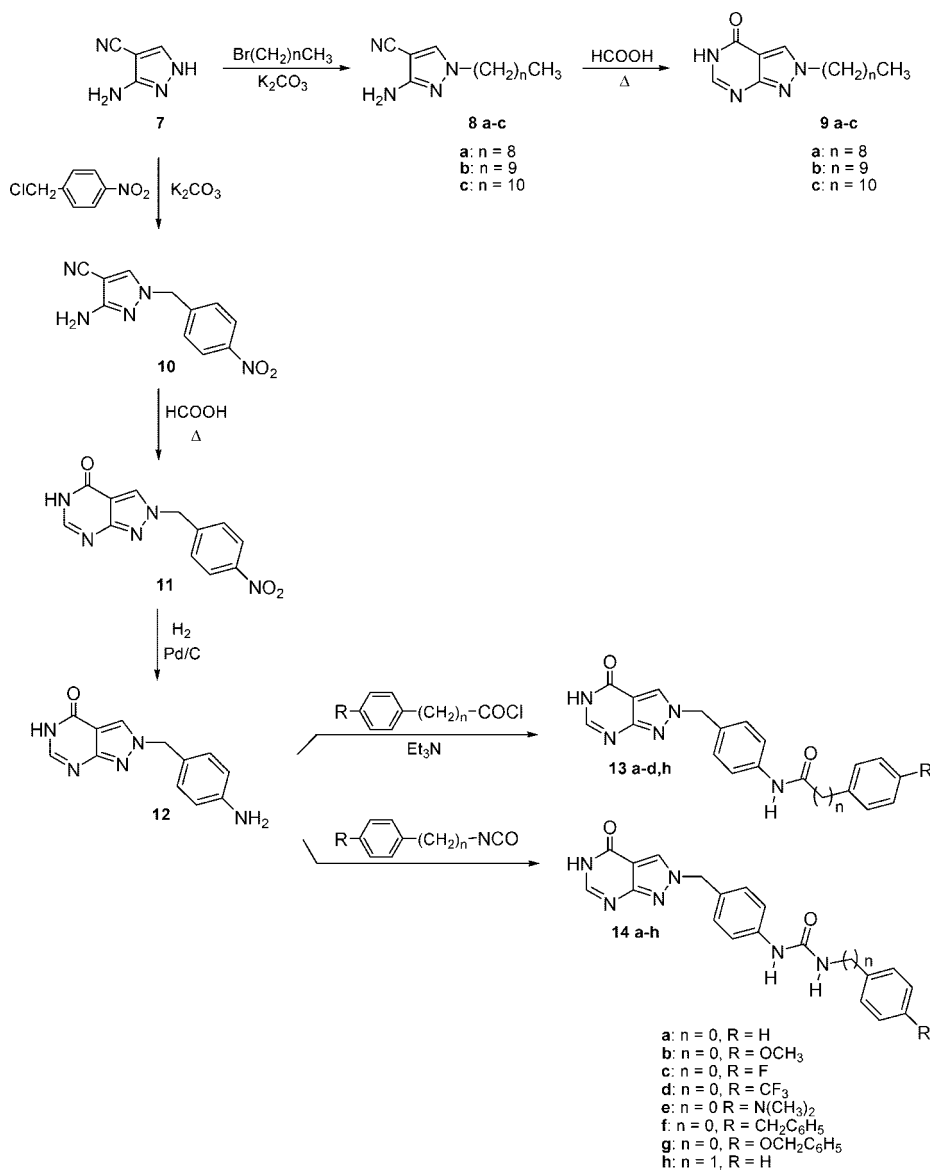
value of 0.51 nM, turned out to be the most potent of the whole subseries, showing a 25-fold gain in activity when compared to **13a**. Finally, an increase in the distance between the phenyl ring and the amide function through a methylene spacer, as in **13h** (K_i = 47.91 nM), was tolerated, as it led to a moderate decrease in activity with respect to **13a**.

Taking into account the favorable results obtained by Terasaka and co-workers through a similar modification on ADA inhibitors,[26] we then replaced the amide linker connecting the two phenyl rings of **13** with an urea residue, thus developing derivatives **14a**−**h**. This structural change led to opposed outcomes. While the unsubstituted urea derivative **14a** (K_i = 2.42 nM) proved to be a more potent inhibitor than the parent amide **14a** (K_i = 12.65 nM), compounds **14b,c**, bearing either an electron-donating group, such as methoxy (**14b**, K_i = 28.27 nM), or an electron-withdrawing substituent, such as fluoro (**14c**, K_i = 1.15 nM), in the para position of the phenyl ring, were less effective than the corresponding **13b,c**. The same was also true for the benzyl derivative **14h** (K_i = 85.7 nM), which showed an almost 2-fold decrease in inhibitory activity when compared to the parent **13h**. In contrast, an opposite trend was shown by compound **14d** (K_i = 0.16 nM), carrying a trifluoromethyl

group: it exhibited a 3-fold increase in efficacy with respect to the amide **13d**, proving it to be the most potent among all the synthesized PPOs. However, it has to be pointed out that, similar to inhibitors **13**, in the subseries **14** the insertion of an electron-withdrawing group in the para position of the distal phenyl ring produced an enhancement in inhibitory potency (compounds **14c** and **14d** with respect to **14a**). A further structure−activity investigation for this class of inhibitors was carried out through the insertion of a dimethylamino group, as in **14e**, a benzyl group, as in **14f**, and a benzyloxy group, as in **14g**. Compound **14e** (K_i = 2.01 nM) resulted a potent ADA inhibitor, showing a K_i value in the nanomolar range, while both derivatives **14f** (K_i = 186.0 nM) and **14g** (K_i = 108.0 nM) displayed a low inhibitory activity in the submicromolar range, thus proving that the substitution pattern, providing an additional aromatic ring, was detrimental against a favorable interaction with the active site of the enzyme.

Pharmacological Evaluation of Compound 14d. The main purpose of our research program was to identify potent ADA inhibitors as novel anti-inflammatory drug candidates. Therefore, we tested the efficacy of the most potent compound **14d** in an

Table 1. ADA Inhibition Data of Derivatives **9a−c**, **13a−e,i**, and **14a−i**

compd	n	R	K_i (nM)[a]
9a	8		na[b]
9b	9		na[b]
9c	10		na[b]
13a	0	H	12.65 ± 1.15
13b	0	OCH_3	15.56 ± 1.52
13c	0	F	0.96 ± 0.081
13d	0	CF_3	0.51 ± 0.042
13h	1	H	47.91 ± 4.13
14a	0	H	2.42 ± 0.19
14b	0	OCH_3	28.27 ± 2.45
14c	0	F	1.15 ± 0.10
14d	0	CF_3	0.16 ± 0.010
14e	0	$N(CH_3)_2$	2.01 ± 0.17
14f	0	$CH_2C_6H_5$	186 ± 16.58
14g	0	$OCH_2C_6H_5$	108 ± 9.70
14h	1	H	85.7 ± 6.60
(+)-EHNA			1.14 ± 0.10

[a] The K_i values are mean values ± SEM. [b] na: nonactive. Inhibition occurred at a concentration higher than 10 μM.

animal model of experimental colitis, induced in rats through administration of DNBS, according to a previously reported protocol.[23]

The test compound, **14d**, was administered ip for 7 days in a dose regimen ranging from 5 to 45 μmol/kg, starting 1 day before the induction of colitis. Its effectiveness was evaluated with respect to dexamethasone, a synthetic glucocorticoid derivative endowed with potent anti-inflammatory activity. At day 6 after colitis induction, a significant body weight loss was recorded: inflamed rats displayed a mean decrease of −20 ± 4.5 g in their body weight, while normal animals showed a weight gain (+25.5 ± 7.5 g) (Figure 1a). A significant reduction in weight loss was observed in animals treated with 45 μmol/kg **14d** (+2.30 ± 2.80 g), while 5 μmol/kg **14d** (−16.50 ± 2.10 g), 15 μmol/kg **14d** (−10.40 ± 1.80 g), and 0.25 μmol/kg dexamethasone were without effects (Figure 1a). Measurement of spleen weight was assumed as an index of systemic inflammation.[29] Treatment with DNBS resulted in a significant increment of spleen weight (+28 ± 4.50%) (Figure 1b). Such an increase was dose-dependently reduced by administration of **14d** (+23.80 ± 4%, +18.90 ± 2.9%, and +10.10 ± 3.6% at 5, 15, 45 μmol/kg, respectively) or dexamethasone (Figure 1b).

Colonic tissues were excised, scored for macroscopic and processed to assess the ability of **14d** to act on parameters related to intestinal inflammation, in particular MDA and TNF-α. The distal colon from DNBS-treated rats appeared thickened and ulcerated with evident areas of transmural inflammation. Adhesions were often present, and the bowel was occasionally dilated, with a macroscopic damage accounting for 7.3 ± 1.5. Rats treated with **14d** displayed a dose-dependent reduction in macroscopic damage score (6.90 ± 1.40 at 5 μmol/kg, 5.60 ± 0.90 at 15 μmol/kg, and 4.30 ± 0.88 at 45 μmol/kg). Dexamethasone-treated animals showed also a significant decrease in macroscopic damage score (Figure 2). MDA levels in colonic tissues from control rats were 157 ± 26.2 μmol/mg. In DNBS-treated animals, a marked increase in MDA concentrations was observed (576 ± 28.1 μmol/mg). Treatments with increasing
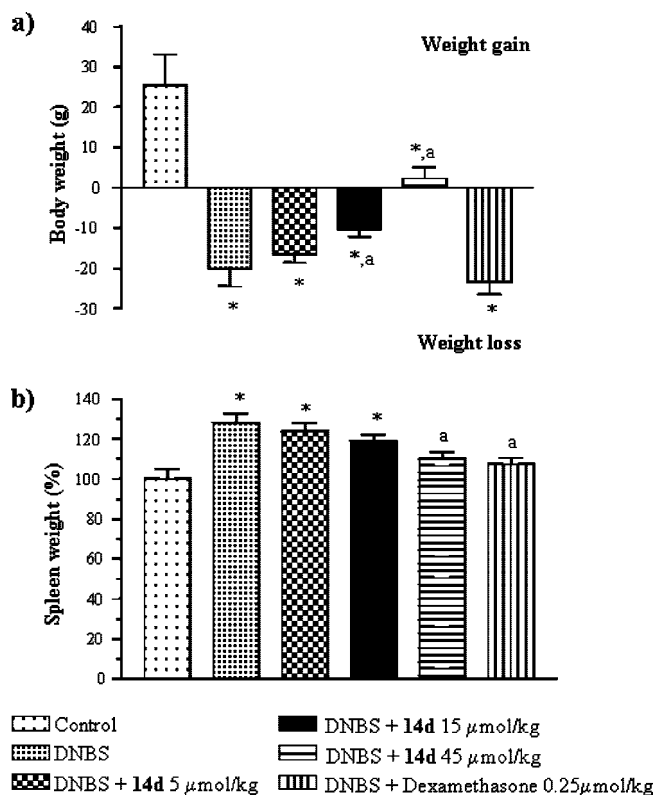

Figure 1. Effects of **14d** (5, 15, and 45 μmol/kg) or dexamethasone (0.25 μmol/kg) on body weight (a) and spleen weight (b) at day 6 after induction of colitis with DNBS in rats. Each column represents the mean ± SEM (n = 6): (*) $p < 0.05$, significant difference vs control group; (a) $p < 0.05$, significant difference vs DNBS group.

doses of **14d** or dexamethasone, 0.25 μmol/kg, significantly attenuated the increase in tissue MDA associated with colitis, although values did not return to basal levels (Figure 3a). Moreover, colonic inflammation induced by DNBS was associated with a significant increase in tissue TNF-α levels (from
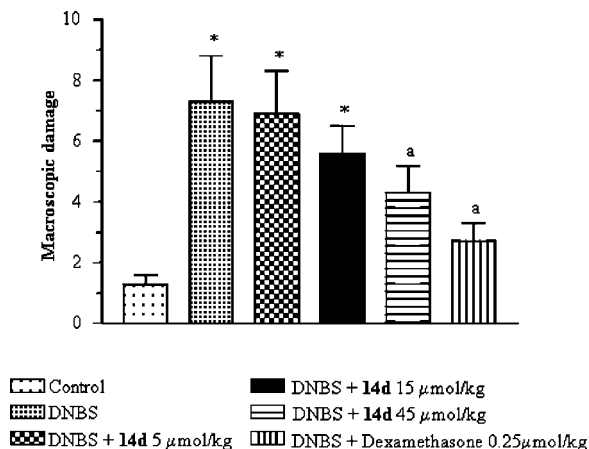
Figure 2. Macroscopic damage scores estimated for colon in rats under normal conditions or following DNBS treatment, either alone or in the presence of **14d** or dexamethasone administration. Each column represents the mean ± SEM ($n = 6$): (*) $p < 0.05$, significant difference vs control group; (a) $p < 0.05$, significant difference vs DNBS group.
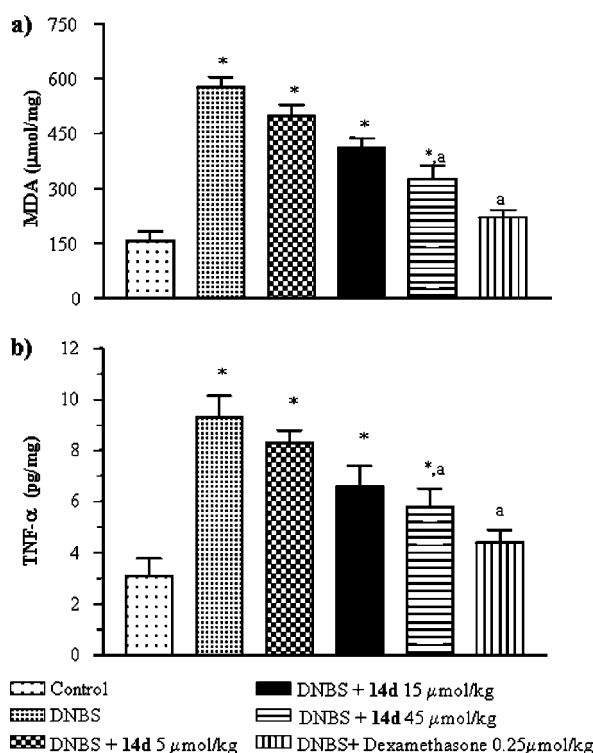

Figure 3. MDA (a) and TNF-α levels (b) in colonic tissues from control rats or in animals treated with DNBS, either alone or in combination with **14d** (5, 15, and 45 μmol/kg) or dexamethasone (0.25 μmol/kg). Each column represents the mean ± SEM ($n = 6$): (*) $p < 0.05$, significant difference vs control rats; (a) $p < 0.05$, significant difference vs DNBS group.

3.1 ± 0.7 to 9.3 ± 0.85 pg/mg). Such an increment was significantly counteracted by 45 μmol/kg **14d** (5.80 ± 0.70 pg/mg) and 0.25 μmol/kg dexamethasone (Figure 3b). These results indicate that treatment with the adenosine deaminase inhibitor **14d** significantly improved both systemic and tissue inflammatory parameters in a dose-dependent fashion. Besides this in vivo anti-inflammatory activity, the tolerability profile of compound **14d** is also a relevant issue, in light of the significant toxicity of other known adenosine deaminase inhibitors, such as CF and dCF.[30,31] In this respect, the present study was not specifically designed and powered to assess toxicological end

points. Nevertheless, following repeated administration of compound **14d**, we could observe that animals displayed normal behavior, and favorable variations in body weight and food intake which, together with a lack of mortality at all doses tested, suggest a good tolerability and encourage further preclinical evaluations, including acute and chronic toxicity. Overall, this novel compound could represent a basis for the development of novel anti-inflammatory drugs with potential therapeutic activity against IBDs.

Docking Studies. To better understand the inhibitory potency of our compounds at a molecolar level and to explain the results obtained from SARs data, a number of PPOs were docked into the publicly available X-ray crystal structure of ADA complexed with the highly potent non-nucleoside inhibitor **6** (PDB code 1O5R).[27]

X-ray studies, performed by different authors, clearly demonstrated that the active site of ADA can adopt two distinct conformations: a closed and an open one (Figure 1 in Supporting Information). In the closed form the active site consists of an hydrophobic subsite, namely, F0, and an hydrophilic area, namely, S0. This latter is perfectly enclosed within a structural gate consisting of the peptide backbone of a β-strand (L182-D185) and two leucine side chains (L58 and L62) from an α-helix (T57-A73). The closed form is usually observed in the complexes with substrate analogues possessing the adenine framework.[32−34] When the structural gate opens, the active site turns into the open form which conserves the closed-form area, consisting of the S0 and F0 subsites, and shows two additional hydrophobic subsites around the gate, defined as F1 and F2.

Comparing crystal structures of apo-ADA and ligated-ADA with various inhibitors, Kinoshita et al.[35,36] hypothesized that removal of a specific water molecule binding at the bottom of the active site might be the trigger of a conformational change from the open to the closed from. While the apo-ADA adopts the open form and the "trigger water" molecule exists at the end of the active site, substrate adenosine or substrate mimic compounds such as HDPR, binding to the hydrophilic S0 subsite, interfere with the water molecule leading to its removal. As a result, the side chain of F65, residing at the α-helix consisting of the active site lid, moves slightly into the active site pocket to occupy the resulting space. This motion causes conformation change of ADA from the open to the closed form, and the interaction between substrate and ADA is increased. Conversely, the non-nucleoside type inhibitors occupy the critical water-binding position, thus causing no significant conformational change of the protein, which remains in the open form. The same is also true for the semitight-binding inhibitor EHNA, whose crystal structure in complex with ADA has been recently published.[36] The adenine nucleus of this inhibitor binds to E217 via two water molecules, thus placing its C8 atom in the "trigger water" binding position.

So far, different experimental structures of various ligands that bind to the binding site of ADA have been deposited in the PDB database[37] (PDB IDs: 1KRM,[38,39] 1NDW, 1NDV, 1NDZ, 1NDY,[27] 1V7A, 1V78, 1V79,[26] 1UML, 1QXL, 1O5R,[27] 2E1W, 1WXZ, 1WXY,[28] 2Z7G,[36] 1ADD,[32,33] and 1A4M[34]). Overlay of the open and closed ADA structures showed that the shape of the active site in the closed form is entirely preserved in the open conformation of the enzyme. For this reason, we chose the open form structure 1O5R,[27] whose cocrystallized ligand (compound **6**) has a phenylurea substructure, which is also present in our ligands.

Docking investigations focused on the most active inhibitors **13a−d**, **14a−d**, **14f**, and **14g**, using the automated docking
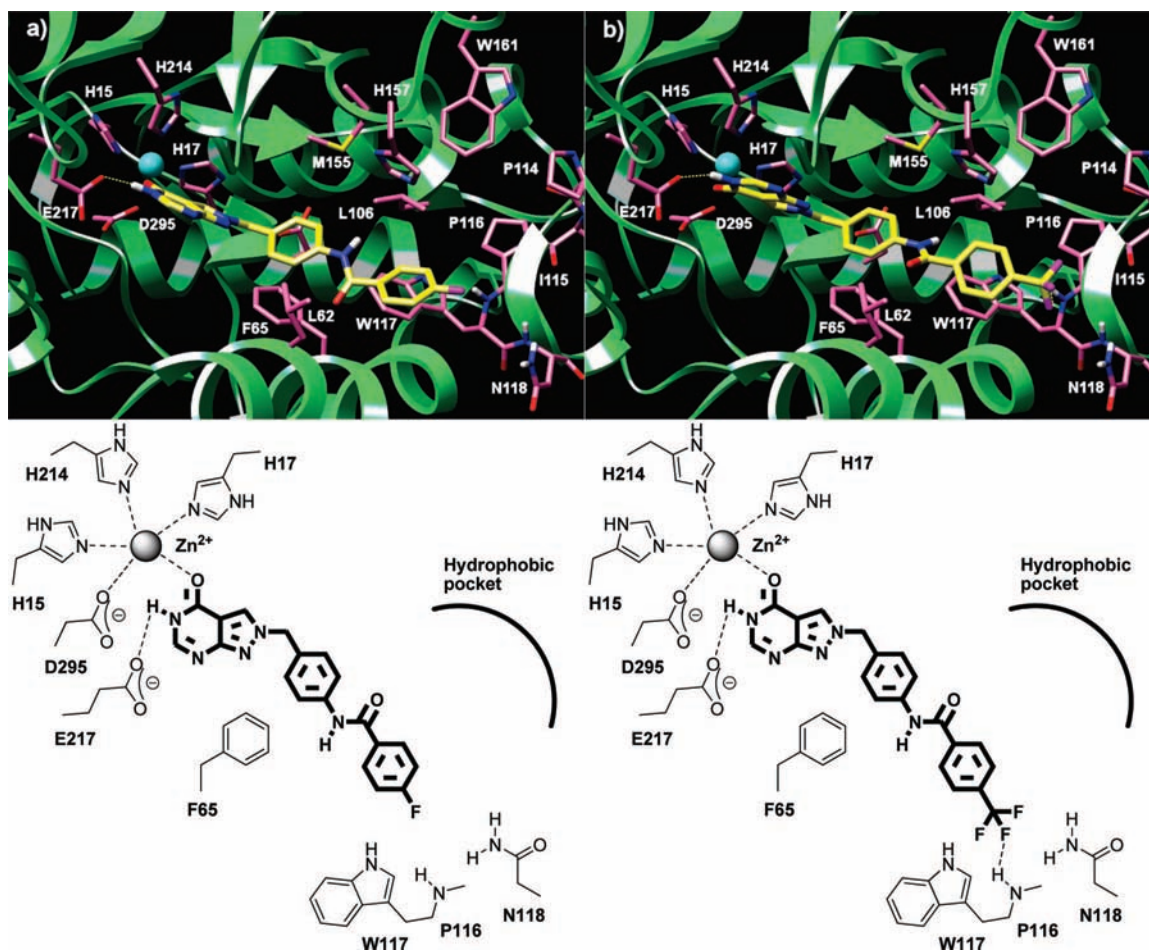
Figure 4. Binding mode of compounds **13c** (a) and **13d** (b) into the ADA binding cavity. Ligands (yellow) and interacting key residues (pink) are represented as stick models, while the enzyme is represented as a green ribbon model. Zinc atom is represented as a cyan ball. H-bonds are shown as dashed yellow lines.

program GOLD, version 4.0,[40,41] which in several studies has been shown to yield better performances compared to other similar programs.[42–45]

Kinoshita et al.[38,39] reported that the D296 side chain is flexible in the active site of ADA; that is, it can adjust to keep the interaction with the respective inhibitor. Accordingly, the side chain of D296 was allowed to move during the docking experiments.

The GoldScore-CS docking protocol[46] was adopted in this study. In this protocol, the poses obtained with the original GoldScore function are rescored and reranked with the GOLD implementation of the ChemScore function.[46,47] To test the validity of this protocol for the bovine ADA system, the cocrystallized ligand (compound **6**) was first docked back into its binding site. In this docking run, the 200 poses produced by GOLD resulted in only one prevailing cluster on the basis of their conformations: 23 of the poses closely resembled the cocrystallized conformation with a heavy atom root-mean-square deviation (rmsd) ranging from 0.6 to 1.8 Å. ChemScore was able to rank 19 out of the 23 poses from this cluster as the highest ranked nineteen poses. Thus, this docking protocol was considered to be suitable for the subsequent docking runs for compounds **13a−d**, **14a−d**, **14f**, and **14g**.

When **13c**, **13d**, **14c**, and **14d** were docked within the ADA active site, about 90% of the conformations generated by GOLD adopted only one highly conserved orientation. The inhibitors entirely occupied the S0 subsite and most of the F0 hydrophobic subsite, but F1 and F2 subsites in the complex remained empty

(Figures 4 and 5). Key interactions stabilized the compounds inside the binding pocket. The pyrazolopyrimidinone C=O oxygen was coordinated to the zinc ion at a distance of 2.5 Å, and its adjacent NH moiety donated a H-bond to the E217 carboxylate group. It is interesting to note that the C=O group on the pyrazolopyrimidinone moiety occupies the same position of the water molecule ligated to and activated by the zinc atom. The diphenylamide or urea chain was localized in a deep and narrow channel at the entrance of the enzyme. Hydrophobic and π−π stacking interactions were found to stabilize the inhibitor/enzyme complexes. The first aromatic system of the urea or amide chain interacted with the lipophilic residues L62 and M155 and, at the same time, formed a face-on-face π−π stacking contact with the F65 aromatic ring. The distal phenyl ring of the same chain was accommodated in a pocket framed by residues L106, P116, W117, H157, and W161, with which it formed hydrophobic interactions. Moreover, the benzo-fused ring of W117 appeared to be optimally oriented for a favorable face-on-face π−π stacking interaction with the distal phenyl ring of amide or urea chain: the planes of the two rings are fairly parallel and separated by a distance ranging between 3.5 and 4.3 Å, respectively. Such an interaction would be consistent with the activity trend of these compounds showing that lipophilic and electron-withdrawing substituents in the para position of the distal aromatic ring increase the potency. In fact, the electron-deficient aromatic ring of **13c**, **13d**, **14c**, and **14d** would more favorably realize the π-stacking charge transfer interactions with the electron-rich benzo-fused ring of W117.
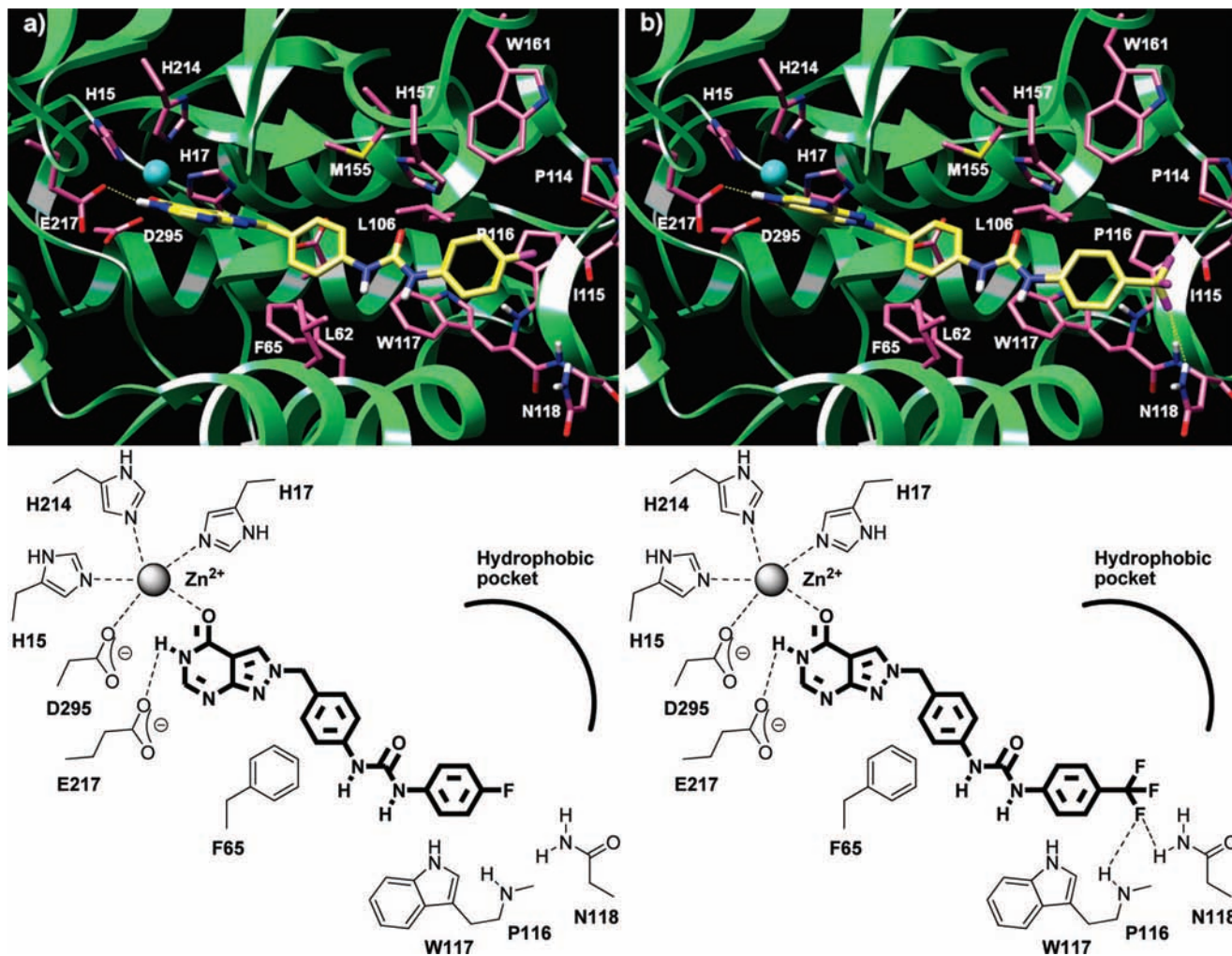
Figure 5. Binding mode of compounds **14c** (a) and **14d** (b) into the ADA binding cavity. Ligands (yellow) and interacting key residues (pink) are represented as stick models, while the enzyme is represented as a green ribbon model. Zinc atom is represented as a cyan ball. H-bonds are shown as dashed yellow lines.

Indeed, visual inspection of the inhibitor/ADA complexes revealed that one CF_3 fluorine atom of **13d** formed a H-bond with NH backbone of P116 (Figure 4b), while the same fluorine atom of **14d** established two H-bonds with both NH backbone and NH_2 side chain of N118 (Figure 5b). The H-bonding capability of the trifluoromethyl group is well-documented in the literature, and several structural studies highlight the evident H-bond acceptor capability in protein−ligand complexes, as assessed by PDB analysis.[48] These results are consistent with the SAR data showing that **13d** and **14d** are the most potent ADA inhibitors of the series with K_i values of 0.51 and 0.16 nM, respectively.

In the most frequently occurring and most favorable docking results, compounds **13b**, **14b**, and **14e** were found to bind in the known binding pocket in a manner similar to the above-described compounds, with the pyrazolopyrimidinone C═O oxygen coordinating the zinc ion and the amide or urea chain localized in a deep and narrow channel at the entrance of the enzyme. However, **13b** and **14b** were weak ADA inhibitors showing K_i values of 15.56 and 28.27 nM, respectively. The reduced activity is probably ascribable to both electronic and steric factors: the *p*-methoxy group, which produces an electron-donating (resonance) effect together with a low withdrawing (inductive) one, could decrease the π−π stacking interaction between W117 and the distal aromatic ring of both **13b** and **14b**. Moreover, the *p*-methoxy group of the longer derivative

14b causes steric hindrance with P114 and I115 C═O backbone, explaining its reduced ADA inhibitory activity.

In light of these results, compound **14e**, which has the electron-donating *p*-dimethylamino substituent on the distal phenyl ring, should be expected to exhibit low inhibitory activity. However, this compound showed a K_i value of 2.01 nM, which is compatible with the decrease in electron-donating power of the *p*-dimethylamino group caused by its protonation at physiological pH. In fact, the protonation of this moiety (using the nitrogen electron lone pair) removes the effect of the lone-pair delocalization.

When the less active **14f** and **14g** were docked within the ADA active site, only 20% of the generated conformations adopted the above-described binding mode, whereas 80% were in a different orientation. The molecules fully occupied the F1, F2, and F0 subsites (Figure 6). The pyrazolopyrimidinone ring and the first aromatic system of the urea chain made hydrophobic interactions with both sides of the hydrophobic gate consisting of the F1 and F2 subsites, while the para-substituted distal aromatic ring of the urea chain fully occupied the hydrophobic F0 subsite. The NH pyrazolopyrimidinone of the inhibitors was involved in a H-bond with the L56 C═O backbone. Interestingly, the inhibitors were positioned far from the active center and did not bind to the hydrophilic S0 subsite at all. These observations plainly explain the loss in the ADA inhibitory potency for **14f** and **14g**.
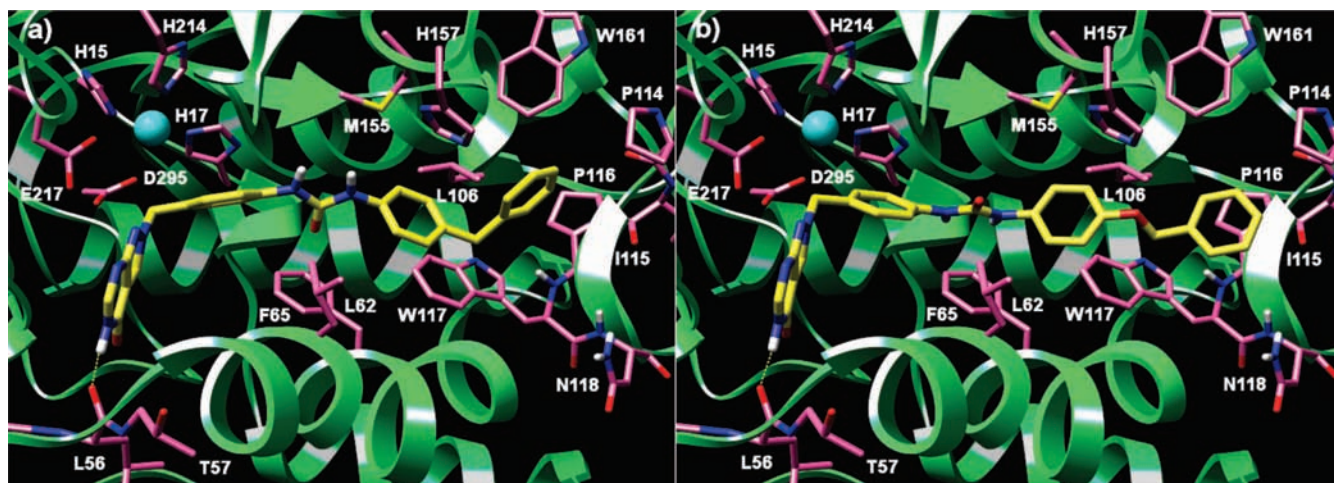
Figure 6. Binding mode of compounds **14f** (a) and **14g** (b) into the ADA binding cavity. Ligands (yellow) and interacting key residues (pink) are represented as stick models, while the enzyme is represented as a green ribbon model. Zinc atom is represented as a cyan ball. H-bonds are shown as dashed yellow lines.

In summary, the most active PPOs proved to interact with the enzyme active site through a direct coordination with the catalytic zinc ion. The mode of binding here proposed is fully substantiated by UV spectroscopy measurements, performed to demonstrate the ability of the pyrazolopyrimidinone ring system to coordinate this metal ion. UV spectra were recorded using derivative **9a** as representative of the whole class. Upon addition of zinc(II) ion to a homogeneous solution of the reference compound, a pronounced decrease in optical density of the absorption maximum was observed (Figure 2 in Supporting Information). An understanding of the binding mode of our inhibitors, fully consistent with the observed SARs, provides a sound platform for a future structure-guided design of novel analogues with higher potency.

Experimental Section

Chemistry. Melting points were determined using a Reichert–Köfler hot-stage apparatus and are uncorrected. Infrared spectra were recorded with a FT-IR spectrometer Nicolet/Avatar in Nujol mulls. Routine ^{1}H NMR spectra were recorded in DMSO-d_6 solution on a Varian Gemini 200 spectrometer operating at 200 MHz. Evaporation was performed in vacuo (rotary evaporator). Anhydrous sodium sulfate was always used as the drying agent. Analytical TLC was carried out on Merck 0.2 mm precoated silica gel aluminum sheets (60 F-254), with visualization by irradiation with a UV lamp. Flash chromatography was performed with Merck silica gel 60 (230–400 mesh ASTM). The microwave-assisted procedures were carried out in sealed vessels using a CEM/Discover LabMate 220VAC/50 Hz microwave system. The UV spectra were measured on a Perkin-Elmer Lambda 25 spectrophotometer at $T = 20$ °C using potassium phosphate buffer, pH 7.2, as solvent and cuvettes with 1 cm path length. Elemental analyses were performed by our analytical laboratory and agreed with theoretical values to within ±0.4%.

The alkyl bromides, the aroyl chlorides, and the isocyanates used to obtain compounds **8a–c**, **13a–d,h**, and **14a–h**, respectively, as well as the 1-(chloromethyl)-4-nitrobenzene, were from Sigma-Aldrich. All other chemicals were of reagent grade.

The 5-amino-1-alkyl-4-pyrazolecarbonitriles **8a–c** were prepared in accordance with previously reported procedures.[22]

General Procedure for the Synthesis of 2-Alkylpyrazolo[3,4-*d*]pyrimidin-4-ones 9a–c. A suspension of 1-alkyl-3-amino-4-pyrazolecarbonitrile **8a–c** (10.0 mmol) in 3 mL of formic acid was vigorously boiled, under stirring, until the disappearance of the starting material (5–8 h, TLC analysis). The cooled solution was then diluted with ice–water, and the solid separated was filtered, washed with water, and recrystallized from the appropriate solvent (Supporting Information, Tables 1 and 2).

3-Amino-1-(4-nitrobenzyl)-4-pyrazolecarbonitrile 10. A solution of 1-(chloromethyl)-4-nitrobenzene (2.05 g, 12.0 mmol) in DMF was added dropwise to a suspension of 3-amino-4-pyrazolecarbonitrile **7** (1.08 g, 10.0 mmol) and anhydrous potassium carbonate (1.66 g, 12.0 mmol) in 25 mL of DMF, and the resulting reaction mixture was stirred at 50 °C for 8 h. After the mixture was cooled, the inorganic material was filtered off and the solution was evaporated to dryness under reduced pressure. The residue was then purified by flash chromatography (eluting system, ethyl acetate/petroleum ether 60–80 °C 7/3) to obtain **10** as a yellow solid, which was recrystallized from ethanol. Yield 67%. Mp: 120–122 °C. IR, ν cm^{-1}: 3390, 3226, 2223, 1639, 1560, 1516. ^{1}H NMR, δ ppm: 5.27 (s, 2H, CH$_2$), 5.66 (s, 2H, NH$_2$, exc), 7.46 (d, 2H, ArH), 8.22 (d, 2H, ArH), 8.31 (s, 1H, H$_5$). Anal. (C$_{11}$H$_9$N$_5$O$_2$) C, H, N.

2-(4-Nitrobenzyl)-2*H*-pyrazolo[3,4-*d*]pyrimidin-4(5*H*)-one 11. A suspension of 3-amino-1-(4-nitrobenzyl)-4-pyrazolecarbonitrile **10** (10.0 mmol) in 3.0 mL of formic acid was vigorously boiled, under stirring, for 5 h. The cooled solution was then diluted with ice–water, and the solid separated was filtered, washed with water, and recrystallized from ethanol. Yield 40%. Mp: 216–218 °C. IR, ν cm^{-1}: 3453, 1692, 1610, 1542. ^{1}H NMR, δ ppm: 5.68 (s, 2H, CH$_2$), 7.56 (d, 2H, ArH), 7.96 (s, 1H, H$_3$), 8.25 (d, 2H, ArH), 8.77 (s, 1H, H$_6$), 11.80 (s, 1H, NH, exc). Anal. (C$_{12}$H$_9$N$_5$O$_3$) C, H, N.

2-(4-Aminobenzyl)-2*H*-pyrazolo[3,4-*d*]pyrimidin-4(5*H*)-one 12. A suspension of 2-(4-nitrobenzyl)-2*H*-pyrazolo[3,4-*d*]pyrimidin-4(5*H*)-one **11** (2.71 g, 10.0 mmol) and 10% palladium on carbon (1.00 mmol) in 250 mL of absolute ethanol was hydrogenated at atmospheric pressure and room temperature until the theoretical uptake of hydrogen was achieved. After the catalyst was filtered, the solvent was evaporated to dryness to give a pale-yellow solid which was collected and recrystallized from ethanol. Yield 95%. Mp: 225–227 °C. IR, ν cm^{-1}: 3409, 3327, 3153, 1700, 1605. ^{1}H NMR, δ ppm: 5.17 (s, 2H, NH$_2$, exc), 5.24 (s, 2H, CH$_2$), 6.53 (d, 2H, ArH), 7.07 (d, 2H, ArH), 7.92 (s, 1H, H$_3$), 8.54 (s, 1H, H$_6$), 11.70 (s, 1H, NH, exc). Anal. (C$_{12}$H$_{11}$N$_5$O) C, H, N.

General Procedure for the Synthesis of *N*-(4-((4-oxo-4,5-dihydropyrazolo[3,4-*d*]pyrimidin-2-yl)methyl)phenyl)arylamides 13a–d,h. 2-(4-Aminobenzyl)-2*H*-pyrazolo[3,4-*d*]pyrimidin-4(5*H*)-one, **12** (2.41 g, 10.0 mmol), the suitable aroyl chloride (12.0 mmol), and triethylamine (1.67 mL, 12.0 mmol) were mixed thoroughly and irradiated with microwaves at 140 °C for 10 min. The cooled residue was then diluted with ice–water and the solid separated was filtered and purified by recrystallization from the appropriate solvent to give the target compounds **13a–d,h** (Supporting Information, Tables 1 and 2).

General Procedure for the Synthesis of 1-(4-((4-Oxo-4,5-dihydropyrazolo[3,4-d]pyrimidin-2-yl)methyl)phenyl)-3-arylureas 14a−h. 2-(4-Aminobenzyl)-2H-pyrazolo[3,4-d]pyrimidin-4(5H)-one **12** (2.41 g, 10.0 mmol) and the suitable isocyanate (12.0 mmol) were mixed thoroughly and irradiated with microwaves at 140 °C for 10 min. The cooled residue was then diluted with toluene and the solid separated was filtered and purified by recrystallization from the appropriate solvent to give the target compounds **14a−h** (Supporting Information, Tables 1 and 2).

Biology. ADA type IX from bovine spleen (150−200 U/mg) and adenosine were purchased from Sigma Chemical Co. All other chemicals were of reagent grade.

Enzymatic Assay. The activity of ADA was determined spectrophotometrically by monitoring for 2 min the change in absorbance at 262 nm, which is due to the deamination of adenosine catalyzed by the enzyme. The change in adenosine concentration/min was determined using a Beckman DU-64 kinetics software program (Solf Pack TM Module). ADA activity was assayed at 30 °C in a reaction mixture containing 50 μM adenosine, 50 mM potassium phosphate buffer, pH 7.2, and 0.3 nM enzyme solution in a total volume of 500 μL. The inhibitory activity of the newly synthesized compounds was assayed by adding 100 μL of the inhibitor solution to the reaction mixture described above. All the inhibitors were dissolved in water, and the solubility was facilitated by using DMSO, whose concentration never exceeded 4% in the final reaction mixture. To correct for the nonenzymatic change in adenosine concentration and the absorption by the test compounds, a reference blank containing all the above assay components except the substrate was prepared. The inhibitory effect of the new derivatives was routinely estimated at a concentration of 10^{-5} M. Those compounds found to be active were tested at additional concentrations between 10^{-5} and 10^{-11} M. Each inhibitor concentration was tested in triplicate, and the determination of the IC_{50} values was performed by linear regression analysis of the log of the concentration response curve. The K_i values were calculated from IC_{50} values by means of the Cheng and Prusoff equation.[49]

Pharmacology. Albino male Sprague−Dawley rats, 250−300 g body weight, were employed throughout the study. The animals were fed standard laboratory chow and tap water ad libitum and were not subjected to experimental procedures for at least 1 week after their delivery to the laboratory. Their care and handling were in accordance with the provisions of the European Union Council Directive 86-609, recognized and adopted by the Italian Government. DNBS and dexamethasone were purchased from Sigma Aldrich (St. Louis, MO). **14d** and dexamethasone were dissolved in sterile dimethyl sulfoxide, and further dilutions were made with sterile saline. The solutions were frozen into aliquots of 2 mL and stored at −80 °C until use.

Induction of Colitis and Drug Treatments. Colitis was induced in accordance with the method previously described by Antonioli et al.[23] Briefly, during a short anesthesia with isoflurane (Abbott, Rome, Italy), an amount of 15 mg of DNBS in 0.25 mL of 50% ethanol was administered intrarectally via a polyethylene PE-60 catheter inserted 8 cm proximal to the anus. Control rats received 0.25 mL of 50% ethanol. Animals underwent subsequent experimental procedures 6 days after DNBS administration to allow a full development of histologically evident colonic inflammation.

Test drugs were administered intraperitoneally for 7 days, starting 1 day before the induction of colitis. Animals were assigned to the following treatment groups, each consisting of six rats: **14d** (5, 15, 45 μmol/kg) or dexamethasone (0.25 μmol/kg). DNBS-untreated animals (control group) and DNBS-treated rats (DNBS group) received drug vehicle to serve as controls. Body weight was monitored daily starting from the onset of drug treatments. To evaluate the anti-inflammatory effects of **14d**, increasing doses of this compound were tested on body weight, spleen weight, macroscopic damage score, tissue TNF-α, and MDA levels in animals with colitis. Dexamethasone was used as comparator drug, and the dose was selected on the basis of previous studies performed on rat models of colitis.[23,50] The macroscopic score was evaluated on the whole colon, whereas biochemical assays were performed on specimens taken from a region of inflamed colon immediately adjacent and distal to the gross necrotic damage.

Assessment of Colitis. At the end of treatments, colonic tissues were excised, rinsed with saline, and scored for macroscopic injury, in accordance with the criteria previously reported by Fornai et al.[51] The macroscopic damage was scored on a 0−6 point scale based on the following criteria: presence of adhesions between colonic tissue and other organs (0 none, 1 minor, 2 major adhesions) and consistency of colonic fecal material (0 formed, 1 loose, 2 liquid stools). All the parameters of macroscopic damage were recorded and scored for each rat by two observers blinded to the treatment. At the time of colitis assessment, the weight of spleen was also measured.

Evaluation of tissue MDA. MDA concentration in colonic specimens was evaluated to obtain quantitative estimation of membrane lipid peroxidation. Colonic tissues were weighed, minced by forceps, homogenized in 2 mL of cold buffer (Tris-HCl, 20 mmol/L, pH 7.4) by a Polytron homogenizer (Cole Palmer homogenizer), and spun by centrifugation at 1500g for 10 min at 4 °C. Colonic MDA concentrations were determined by means of a kit for colorimetric assay (Calbiochem-Novabiochem Corporation, San Diego, CA), and the results were expressed as μmol of MDA per mg of colonic tissue.

TNF-α Assay. Tissue TNF-α levels were measured using a kit for enzyme-linked immunosorbent assay (Biosource International, Camarillo, CA). For this purpose, as described by Marquez et al.,[52] tissue samples, previously stored at −80 °C, were weighed, thawed, and homogenized in 0.3 mL of phosphate buffered saline (pH 7.2)/100 mg of tissue at 4 °C and centrifuged at 13400g for 20 min. One hundred microliter aliquots of the supernatants were then used for assay. Tissue TNF-α levels were expressed as picogram per milligram of tissue.

Statistical Analysis. The results are given as the mean ± standard error of the mean (SEM). The statistical significance of data was evaluated by one way analysis of variance (ANOVA) followed by post hoc analysis by Student−Newman−Keuls test, and P values lower than 0.05 were considered significant. All statistical procedures were performed using GraphPad Prism, version 3.0, software (GraphPad, San Diego, CA).

Computational Chemistry. Molecular modeling and graphic manipulations were performed using the molecular operating environment (MOE)[53] and UCSF-CHIMERA[54] software packages running on a 2 CPU (PIV 2.0−3.0 GHz) Linux workstation. Energy minimizations were realized by employing the AMBER, version 9, program,[55] selecting the Cornell et al. force field.[56]

Ligand and Protein Setup. The core structures of compounds **13a−d**, **14a−d,f,g** were constructed using standard bond lengths and bond angles of the MOE fragment library. Geometry optimizations were accomplished with the MMFF94X force field,[57−61] available within MOE. The crystal structure of the bovine ADA complexed with the highly potent non-nucleoside inhibitor **6** (PDB code 1O5R)[27] recovered from Brookhaven Protein Database[37] was used for the docking experiments. Bound ligand and water molecules were removed. A correct atom assignment for Asn, Gln, and His residues was done, and hydrogen atoms were added using standard MOE geometries. Partial atomic charges were computed by MOE using the Amber99 force field.

Docking Simulations. Docking of **13a−d**, **14a−d,f,g** to ADA was performed with GOLD, version 4,0,[40] which uses a genetic algorithm for determining the docking modes of ligands and proteins. An advantage of GOLD over other docking methods is the program's ability to account for some rotational protein flexibility, as well as full ligand flexibility. Specifically, OH groups of S, T, and Y and amino groups of K are allowed to rotate during docking to optimize H-bonding to the ligand. GOLD requires a user-defined binding site. It searches for a cavity within the defined area and considers all the solvent-accessible atoms in that area as active-site atoms. The fitness score function that was implemented in GOLD (GOLDScore) is made up of four components that account for protein−ligand binding energy: protein−ligand hydrogen bond energy (external H-bond), protein−ligand van der Waals

energy (external vdw), ligand internal vdw energy (internal vdw), and ligand torsional strain energy (internal torsion). Parameters used in the fitness function (hydrogen bond energies, atom radii, polarizabilities, torsion potentials, hydrogen bond directionalities, and so forth) are taken from the GOLD parameter file. The fitness score is taken as the negative of the sum of the energy terms, so larger fitness scores indicated better bindings. The fitness function has been optimized for the prediction of ligand binding positions rather than the prediction of binding affinities, although some correlation with the latter can also be found.[46] The protein input file may be the entire protein structure or a part of it comprising only the residues that are in the region of the ligand binding site. In the present study, GOLD was allowed to calculate interaction energies within a sphere of a 7 Å radius centered on the cocrystal compound **6** in the ADA structure. The Goldscore-CS docking protocol[46] was adopted in this study. In this protocol, the poses obtained with the original Goldscore function are rescored and reranked with the GOLD implementation of the CHEMscore function.[46,47] The mobility of D296 side chain was set up using the FLEXIBLE SIDECHAINS option in the GOLD front end, which incorporates the rotamer library reported by Lovell et al.[62] To perform a thorough and unbiased search of the conformation space, each docking run was allowed to produce 200 poses without the option of early termination, using standard default settings. The top solution obtained after reranking of the poses with CHEMscore was selected to generate the ADA/inhibitor complexes.

Energy Refinement of the Ligand/Enzyme Complexes. To eliminate any residual geometric strain, the obtained complexes were energy minimized for 5000 steps using combined steepest descent and conjugate gradient methods until a convergence value of 0.001 kcal/(mol·Å). The zinc divalent cation in the ADA crystal structure was replaced by the tetrahedron-shaped zinc divalent cation that has four cationic dummy atoms surrounding the central zinc ion,[63] without resorting to the use of a covalent bond between zinc and its coordinate[64-66] or to semiempirical calculations.[67] This approach uses four identical dummy atoms tetrahedrically attached to the zinc ion and transfers all the atomic charge of the zinc divalent cation evenly to the four dummy atoms. The four peripheral atoms are "dummy" in that they interact with other atoms electrostatically but not sterically, thus mimicking zinc's $4s4p^3$ vacant orbitals that accommodate the lone-pair electrons of zinc coordinates. H15, H17, H214, and D295, which are the first-shell zinc coordinates, were treated as histidinate (HIN) and aspartate (ASP).[63,68-71] D181 and E260, which form a H-bond with His214 and His15, respectively, were treated as glutamic acid (GLH). Upon minimization, the protein backbone atoms were held fixed. Geometry optimizations were performed using the SANDER module in the AMBER suite of programs, employing the Cornell et al. force field to assign parameters for the standard amino acids. General AMBER force field (GAFF) parameters were assigned to ligands, while the published force field parameters were used for the tetrahedron-shaped zinc divalent cation.[72] The partial charges were calculated using the AM1-BCC method as implemented in the ANTECHAMBER suite of AMBER.

UV Absorption Spectroscopic Analyses. Stock solutions of 100.0 μM ZnCl$_2$, from Sigma-Aldrich, and of 50.00 μM **9a** were prepared by dissolving the required amount of substance in distilled water. For **9a** the solubility was facilitated by using DMSO. Metal coordination experiments were carried out by adding from 0 to 2.0 mL of zinc(II) ion solution, in 0.5 mL increments, to 2.0 mL of 50.00 μM **9a** and diluting to a total volume of 5.0 mL with potassium phosphate, pH 7.2. Titration was monitored by UV–vis spectroscopy measuring the absorbance of each solution, at λ ranging from 190 to 260 nm and at $T = 20$ °C, using a PerkinElmer Lambda 25 spectrophotometer.

Supporting Information Available: Tables of physical, spectral, and analytical data of compounds described; figures showing the closed and open forms of ADA and UV absorption spectra of compound **9a**. This material is available free of charge via the Internet at http://pubs.acs.org.

References

(1) Cristalli, G.; Costanzi, S.; Lambertucci, C.; Lupidi, G.; Vittori, S.; Volpini, R.; Campioni, E. Adenosine Deaminase: Functional Implications and Different Classes of Inhibitors. *Med. Res. Rev.* **2001**, *21*, 105–128.

(2) Yegutkin, G. G. Nucleotide- and Nucleoside-Converting Ectoenzymes: Important Modulators of Purinergic Signalling Cascade. *Biochim. Biophys. Acta, Mol. Cell Res.* **2008**, *1783*, 673–694.

(3) Franco, R.; Mallol, J.; Casado, V.; Lluis, C.; Canela, E. I.; Saura, C.; Blanco, J.; Ciruela, F. Ecto-Adenosine Deaminase: An Ecto-Enzyme and a Costimulatory Protein Acting on a Variety of Cell Surface Receptors. *Drug Dev. Res.* **1998**, *45*, 261–268.

(4) Franco, R.; Valenzuela, A.; Lluis, C.; Blanco, J. Enzymatic and Extraenzymatic Role of Ecto-Adenosine Deaminase in Lymphocytes. *Immunol. Rev.* **1998**, *161*, 27–42.

(5) Aldrich, M. B.; Blackburn, M. R.; Kellems, R. E. The Importance of Adenosine Deaminase for Lymphocyte Development and Function. *Biochem. Biophys. Res. Commun.* **2000**, *272*, 311–315.

(6) Chen, T.; Smyth, T.; Abbott, C. A. CD26. *J. Biol. Regul. Homeostatic Agents* **2004**, *181*, 47–54.

(7) Blackburn, M. R.; Kellems, R. E. Adenosine Deaminase Deficiency: Metabolic Basis of Immune Deficiency and Pulmonary Inflammation. *Adv. Immunol.* **2005**, *86*, 1–41.

(8) Hershfield, M. S. New Insights into Adenosine-Receptor-Mediated Immunosuppression and the Role of Adenosine in Causing the Immunodeficiency Associated with Adenosine Deaminase Deficiency. *Eur. J. Immunol.* **2005**, *35*, 25–30.

(9) Resta, R.; Thompson, L. F. SCID: The Role of Adenosine Deaminase Deficiency. *Immunol. Today* **1997**, *18*, 371–374.

(10) Hershfield, M. S. Adenosine Deaminase Deficiency: Clinical Expression, Molecular Basis, and Therapy. *Semin Hematol.* **1998**, *35*, 291–298.

(11) Sauter, C.; Lamanna, N.; Weiss, M. A. Pentostatin in Chronic Lymphocytic Leukemia. *Expert Opin. Drug Metab. Toxicol.* **2008**, *4*, 1217–1222.

(12) Honma, Y. A Novel Therapeutic Strategy Against Monocytic Leukemia with Deoxyadenosine Analogs and Adenosine Deaminase Inhibitors. *Leuk. Lymphoma* **2001**, *42*, 953–962.

(13) Robak, T.; Korycka, A.; Kasznicki, M.; Wrzesien-Kus, A.; Smolewski, P. Purine Nucleoside Analogues for the Treatment of Hematological Malignancies: Pharmacology and Clinical Applications. *Curr. Cancer Drug Targets* **2005**, *5*, 421–444.

(14) Köse, K.; Utaş, S.; Yazici, C.; Akdaş, A.; Keleştimur, F. Effect of Propylthiouracil on Adenosine Deaminase Activity and Thyroid Function in Patients with Psoriasis. *Br. J. Dermatol.* **2001**, *144*, 1121–1126.

(15) Cronstein, B. N. Adenosine: An Endogenous Anti-Inflammatory Agent. *J. Appl. Physiol.* **1994**, *76*, 5–13.

(16) Ohta, A.; Sitkovsky, M. Role of G-Protein-Coupled Adenosine Receptors in Down-Regulation of Inflammation and Protection from Tissue Damage. *Nature* **2001**, *414*, 916–920.

(17) Haskó, G.; Deitch, E. A.; Szabo, C.; Nemeth, Z. H.; Vizi, E. S. Adenosine: A Potential Mediator of Immunosuppression in Multiple Organ Failure. *Curr. Opin. Pharmacol.* **2002**, *2*, 440–444.

(18) Haskó, G.; Cronstein, B. N. Adenosine: An Endogenous Regulator of Innate Immunity. *Trends Immunol.* **2004**, *25*, 33–39.

(19) Cha, S.; Agarwal, R. P.; Parks, R. E., Jr. Thigh-Binding Inhibitors. II. Non-Steady-State Nature of Inhibition of Milk Xantine Oxidase by Allopurinol and Alloxanthine and of Human Erythrocytic Adenosine Deaminase by Coformicin. *Biochem. Pharmacol.* **1975**, *24*, 2187–2197.

(20) Agarwal, R. P.; Spector, T.; Parks, R. E., Jr. Thigh-Binding Inhibitors. IV. Inhibition of Adenosine Deaminase by Various Inhibitors. *Biochem. Pharmacol.* **1977**, *26*, 359–367.

(21) Schaeffer, H. J.; Schwender, C. F. Enzyme Inhibitors. 26. Bridging Hydrophobic and Hydrophilic Regions of Adenosine Deaminase with Some 9-(2-Hydroxy-3-alkyl)adenines. *J. Med. Chem.* **1974**, *17*, 6–8.

(22) Da Settimo, F.; Primofiore, G.; La Motta, C.; Taliani, S.; Simorini, F.; Marini, A. M.; Mugnaini, L.; Lavecchia, A.; Novellino, E.; Tuscano, D.; Martini, C. Novel, Highly Potent Adenosine Deaminase Inhibitors Containing the Pyrazolo[3,4-*d*]pyrimidine Ring System. Synthesis, Structure–Activity Relationships, and Molecular Modeling Studies. *J. Med. Chem.* **2005**, *48*, 5162–5174.

(23) Antonioli, L.; Fornai, M.; Colucci, R.; Ghisu, N.; Da Settimo, F.; Natale, G.; Kastsiuchenka, O.; Duranti, E.; Virdis, A.; Vassalle, C.; La Motta, C.; Mugnaini, L.; Breschi, M. C.; Blandizzi, C.; Del Tacca, M. Inhibition of Adenosine Deaminase Attenuates Inflammation in Experimental Colitis. *J. Pharmacol. Exp. Ther.* **2007**, *322*, 435–442.

(24) Terasaka, T.; Nakanishi, I.; Nakamura, K.; Eikyu, Y.; Kinoshita, T.; Nishio, N.; Sato, A.; Kuno, M.; Seki, N.; Sakane, K. Structure-Based de Novo Design of Non-Nucleoside Adenosine Deaminase Inhibitors. *Bioorg. Med. Chem. Lett.* **2003**, *13*, 1115–1118.

(25) Terasaka, T.; Kinoshita, T.; Kuno, M.; Nakanishi, I. A Highly Potent Non-Nucleoside Adenosine Deaminase Inhibitor: Efficient Drug Discovery by Intentional Lead Hybridization. *J. Am. Chem. Soc.* **2004**, *126*, 34–35.

(26) Terasaka, T.; Okumura, H.; Tsuji, K.; Kato, T.; Nakanishi, I.; Kinoshita, T.; Kato, Y.; Kuno, M.; Seki, N.; Naoe, Y.; Inoue, T.; Tanaka, K.; Nakamura, K. Structure-Based Design and Synthesis of Non-Nucleoside, Potent, and Orally Bioavailable Adenosine Deaminase Inhibitors. *J. Med. Chem.* **2004**, *47*, 2728–2731.

(27) Terasaka, T.; Kinoshita, T.; Kuno, M.; Seki, N.; Tanaka, K.; Nakanishi, I. Structure-Based Design, Synthesis, and Structure–Activity Relationship Studies of Novel Non-Nucleoside Adenosine Deaminase Inhibitors. *J. Med. Chem.* **2004**, *47*, 3730–3743.

(28) Terasaka, T.; Tsuji, K.; Kato, T.; Nakanishi, I.; Kinoshita, T.; Kato, Y.; Kuno, M.; Inoue, T.; Tanaka, K.; Nakamura, K. Rational Design of Non-Nucleoside, Potent, and Orally Bioavailable Adenosine Deaminase Inhibitors: Predicting Enzyme Conformational Change and Metabolism. *J. Med. Chem.* **2005**, *48*, 4750–4753.

(29) Siegmund, B.; Rieder, F.; Albrich, S.; Wolf, K.; Bidlingmaier, C.; Firestein, G. S.; Boyle, D.; Lehr, H. A.; Loher, F.; Hartmann, G.; Endres, S.; Eigler, A. Adenosine Kinase Inhibitor GP515 Improves Experimental Colitis in Mice. *J. Pharmacol. Exp. Ther.* **2001**, *296*, 99–105.

(30) Robak, T. Therapy of Chronic Lymphocytic Leukaemia with Purine Nucleoside Analogues: Facts and Controversies. *Drugs Aging* **2005**, *22*, 983–1012.

(31) Sauter, C.; Lamanna, N.; Weiss, M. A. Pentostatin in Chronic Lymphocytic Leukemia. *Expert Opin. Drug Metab. Toxicol.* **2008**, *4*, 1217–22.

(32) Wilson, D. K.; Rudolph, F. B.; Quiocho, F. A. Atomic Structure of Adenosine Deaminase Complexed with a Transition State Analog: Understanding Catalysis and Immunodeficiency Mutation. *Science* **1991**, *252*, 1278–1284.

(33) Wilson, D. K.; Quiocho, F. A. A Pre-Transition-State Mimic of an Enzyme: X-ray Structure of Adenosine Deaminase with Bound 1-Deazaadenosine and Zinc Activated Water. *Biochemistry* **1993**, *32*, 1689–1694.

(34) Wang, Z.; Quiocho, F. A. Complexes of Adenosine Deaminase with Two Potent Inhibitors: X-ray Structures in Four Independent Molecules at pH of Maximum Activity. *Biochemistry* **1998**, *37*, 8314–8324.

(35) Kinoshita, T.; Nakanishi, I.; Terasaka, T.; Kuno, M.; Seki, N.; Warizaya, M.; Matsumura, H.; Inoue, T.; Takano, K.; Adachi, H.; Mori, Y.; Fujii, T. Structural Basis of Compound Recognition by Adenosine Deaminase. *Biochemistry* **2005**, *44*, 10562–10569.

(36) Kinoshita, T.; Tada, T.; Nakanishi, I. Conformational Change of Adenosine Deaminase during Ligand-Exchange in a Crystal. *Biochem. Biophys. Res. Commun.* **2008**, *373*, 53–57.

(37) Berman, H. M.; Westbrook, J.; Feng, Z.; Gilliland, G.; Bhat, T. N.; Weissig, H.; Shindyalov, I. N.; Bourne, P. E. The Protein Data Bank. *Nucleic Acids Res.* **2000**, *28*, 235–242.

(38) Kinoshita, T.; Nishio, N.; Sato, A.; Murata, M. Crystallization and Preliminary Analysis of Bovine Adenosine Deaminase. *Acta Crystallogr.* **1999**, *D55*, 2031–2032.

(39) Kinoshita, T.; Nishio, N.; Nakanishi, I.; Sato, A.; Fujii, T. Crystal Structure of Bovine Adenosine Deaminase Complexed with 6-Hydroxy-1,6-dihydropurine Riboside. *Acta Crystallogr.* **2003**, *D59*, 299–303.

(40) GOLD, version 4.0; CCDC Software Limited: Cambridge, U.K., 2008.

(41) Jones, G.; Willett, P.; Glen, R. C.; Leach, A. R.; Taylor, R. Development and Validation of a Genetic Algorithm for Flexible Docking. *J. Mol. Biol.* **1997**, *267*, 727–748.

(42) Schulz-Gasch, T.; Stahl, M. Binding Site Characteristics in Structure-Based Virtual Screening: Evaluation of Current Docking Tools. *J. Mol. Model.* **2003**, *9*, 47–57.

(43) Wang, R.; Lu, Y.; Wang, S. Comparative Evaluation of 11 Scoring Functions for Molecular Docking. *J. Med. Chem.* **2003**, *46*, 2287–2303.

(44) Kellenberger, E.; Rodrigo, J.; Muller, P.; Rognan, D. Comparative Evaluation of Eight Docking Tools for Docking and Virtual Screening Accuracy. *Proteins: Struct., Funct., Bioinf.* **2004**, *57*, 225–242.

(45) Warre, G. L.; Andrews, C. W.; Capelli, A. M.; Clarke, B.; LaLonde, J.; Lambert, M. H.; Lindvall, M.; Nevins, N.; Semus, S. F.; Senger, S.; Tedesco, G.; Wall, I. D.; Woolven, J. M.; Peishoff, C. E.; Head, M. S. A Critical Assessment of Docking Programs and Scoring Functions. *J. Med. Chem.* **2006**, *49*, 5912–5931.

(46) Verdonk, M. L.; Cole, J. C.; Hartshorn, M. J.; Murray, C. W.; Taylor, R. D. Improved Protein−Ligand Docking Using GOLD. *Proteins: Struct., Funct., Genet.* **2003**, *52*, 609–623.

(47) Eldridge, M. D.; Murray, C. W.; Auton, T. R.; Paolini, G. V.; Mee, R. P. Empirical Scoring Functions: i. The Development of a Fast Empirical Scoring Function To Estimate the Binding Affinity of Ligands in Receptor Complexes. *J. Comput.-Aided Mol. Des.* **1997**, *11*, 425–445.

(48) Carosati, E.; Sciabola, S.; Cruciani, G. Hydrogen Bonding Interactions of Covalently Bonded Fluorine Atoms: From Crystallographic Data to a New Angular Function in the GRID Force Field. *J. Med. Chem.* **2004**, *47*, 5114–5125.

(49) Cheng, Y. C.; Prusoff, W. H. Relation Between Inhibition Constant K_i and the Concentration of Inhibitor Which Causes Fifty Percent Inhibition (IC_{50}) of an Enzymatic Reaction. *Biochem. Pharmacol.* **1973**, *22*, 3099–3108.

(50) Nakase, H.; Okazaki, K.; Tabata, Y.; Uose, S.; Ohana, M.; Uchida, K.; Nishi, T.; Debreceni, A.; Itoh, T.; Kawanami, C.; Iwano, M.; Ikada, Y.; Chiba, T. An Oral Drug Delivery System Targeting Immune-Regulating Cells Ameliorates Mucosal Injury in Trinitrobenzene Sulfonic Acid-Induced Colitis. *J. Pharmacol. Exp. Ther.* **2001**, *297*, 1122–1128.

(51) Fornai, M.; Blandizzi, C.; Antonioli, L.; Colucci, R.; Bernardini, N.; Segnani, C.; De Ponti, F.; Del Tacca, M. Differential Role of Cyclooxygenase 1 and 2 Isoforms in the Modulation of Colonic Neuromuscular Function in Experimental Inflammation. *J. Pharmacol. Exp. Ther.* **2006**, *317*, 938–945.

(52) Marquez, E.; Sanchez-Fidalgo, S.; Calvo, J. R.; de la Lastra, C. A.; Motilva, V. Acutely Administered Melatonin Is Beneficial While Chronic Melatonin Treatment Aggravates the Evolution of TNBS-Induced Colitis. *J. Pineal Res.* **2006**, *40*, 48–55.

(53) *Molecular Operating Environment (MOE)*, version 2005.06; Chemical Computing Group, Inc.: Montreal, Canada, 2005.

(54) Huang, C. C.; Couch, G. S.; Pettersen, E. F.; Ferrin, T. E. Chimera: An Extensible Molecular Modelling Application Constructed Using Standard Components. *Pac. Symp. Biocomput.* **1996**, *1*, 724. (http://www.cgl.ucsf.edu/chimera).

(55) Case, D. A.; Darden, T. A.; Cheatham, T. E., III; Simmerling, C. L.; Wang, J.; Duke, R. E.; Luo, R.; Merz, K. M.; Pearlman, D. A.; Crowley, M.; Walker, R. C.; Zhang, W.; Wang, B.; Hayik, S.; Roitberg, A.; Seabra, G.; Wong, K. F.; Paesani, F.; Wu, X.; Brozell, S.; Tsui, V.; Gohlke, H.; Yang, L.; Tan, C.; Mongan, J.; Hornak, V.; Cui, G.; Beroza, P.; Mathews, D. H.; Schafmeister, C.; Ross, W. S.; Kollman, P. A. *AMBER*, version 9; University of California: San Francisco, CA, 2006.

(56) Cornell, W. D.; Cieplak, P.; Bayly, C. I.; Gould, I. R.; Merz, K. M.; Ferguson, D. M.; Spellmeyer, D. C.; Fox, T.; Caldwell, J. W.; Kollman, P. A. A Second Generation Force Field for the Simulation of Proteins, Nucleic Acids, and Organic Molecules. *J. Am. Chem. Soc.* **1995**, *117*, 5179–5197.

(57) Halgren, T. A. Merck Molecular Force Field. I. Basis, Form, Scope, Parameterization, and Performance of MMFF94. *J. Comput. Chem.* **1996**, *17*, 490–512.

(58) Halgren, T. A. Merck Molecular Force Field. II. MMFF94 van der Waals and Electrostatic Parameters for Intermolecular Interactions. *J. Comput. Chem.* **1996**, *17*, 520–552.

(59) Halgren, T. A. Merck Molecular Force Field. III. Molecular Geometries and Vibrational Parameters for Intermolecular Interactions. *J. Comput. Chem.* **1996**, *17*, 553–586.

(60) Halgren, T. A. Merck Molecular Force Field. IV. Conformational Energies and Geometries for MMFF94. *J. Comput. Chem.* **1996**, *17*, 587–615.

(61) Halgren, T. A. Merck Molecular Force Field. V. Extension of MMFF94 Using Experimental Data, Additional Computational Data, and Empirical Rules. *J. Comput. Chem.* **1996**, *17*, 616–641.

(62) Lovell, S. C.; Word, J. M.; Richardson, J. S.; Richardson, D. C. The Penultimate Rotamer Library. *Proteins* **2000**, *40*, 389–408.

(63) Pang, Y. P. Novel Zinc Protein Molecular Dynamics Simulations: Steps Toward Antiangiogenesis for Cancer Treatment. *J. Mol. Model.* **1999**, *5*, 196–202.

(64) Hoops, S. C.; Anderson, K. W.; Merz, K. M. J. Force Field Design for Metalloproteins. *J. Am. Chem. Soc.* **1991**, *113*, 8262–8270.

(65) Ryde, U. Molecular Dynamics Simulations of Alcohol Dehydrogenase with a Four- or Five-Coordinate Catalytic Zinc Ion. *Proteins* **1995**, *21*, 40–56.

(66) Lu, D. S.; Voth, G. A. Molecular Dynamics Simulations of Human Carbonic Anhydrase II: Insight into Experimental Results and the Role of Solvation. *Proteins* **1998**, *33*, 119–134.

(67) Berweger, C. D.; Thiel, W.; van Gunsteren, W. F. Molecular-Dynamics Simulation of the Beta Domain of Metallothionein with a Semiempirical Treatment of the Metal Core. *Proteins* **2000**, *41*, 299–315.

(68) Pang, Y. P.; Xu, K.; El Yazal, J.; Prendergast, F. G. Successful Molecular Dynamics Simulation of the Zinc-Bound Farnesyltransferase Using the Cationic Dummy Atom Approach. *Protein Sci.* **2000**, *9*, 1857–1865.

(69) El Yazal, J.; Pang, Y. P. Ab Initio Calculations of Proton Dissociation Energies of Zinc Ligands: Hypothesis of Imidazolate as Zinc Ligand in Proteins. *J. Phys. Chem. B* **1999**, *103*, 8773–8779.

(70) El Yazal, J.; Roe, R. R.; Pang, Y. P. Zinc's Affect on Proton Transfer between Imidazole and Acetate Predicted by ab Initio Calculations. *J. Phys. Chem. B* **2000**, *104*, 6662–6667.

(71) El Yazal, J.; Pang, Y. P. Comparison of DFT, Moller−Plesset, and Coupled Cluster Calculations of the Proton Dissociation Energies of Imidazole and *N*-Methylacetamide in the Presence of Zinc(II). *J. Mol. Struct.: THEOCHEM* **2001**, *545*, 271–274.

(72) Pang, Y. P. Successful Molecular Dynamics Simulation of Two Zinc Complexes Bridged by a Hydroxide in Phosphotriesterase Using the Cationic Dummy Atom Method. *Proteins* **2001**, *45*, 183–189.